Leng *et al.*
Chinese Journal of Mechanical Engineering (2025) 38:102
https://doi.org/10.1186/s10033-025-01270-2

Chinese Journal of Mechanical Engineering

ORIGINAL ARTICLE

Open Access

Multi-mode Evasion Assistance Control Method for Intelligent Distributed-drive Electric Vehicle Considering Human Driver's Reaction

Bo Leng[1], Zhuoren Li[1*], Ming Liu[1], Ce Yang[1], Yi Luo[2], Amir Khajepour[3] and Lu Xiong[1]

Abstract

Vehicle collision avoidance (CA) has been widely studied to improve road traffic safety. However, most evasion assistance control methods face challenges in effectively coordinating collision avoidance safety and human-machine interaction conflict. This paper introduces a novel multi-mode evasion assistance control (MEAC) method for intelligent distributed-drive electric vehicles. A reference safety area is established considering the vehicle safety and stability requirements, which serves as a guiding principle for evading obstacles. The proposed method includes two control modes: Shared-EAC (S-EAC) and Emergency-EAC (E-EAC). In S-EAC, an integrated human-machine authority allocation mechanism is designed to mitigate conflicts between human drivers and the control system during collision avoidance. The E-EAC mode is tailored for situations where the driver has no collision avoidance behavior and utilizes model predictive control to generate additional yaw moments for collision avoidance. Simulation and experimental results indicate that the proposed method reduces human-machine conflict and assists the driver in safe collision avoidance in the S-EAC mode under various driver conditions. In addition, it enhances the vehicle responsiveness and reduces the extent of emergency steering in the E-EAC mode while improving the safety and stability during the collision avoidance process.

Keywords Intelligent vehicles, Distributed-drive electric vehicle, Collision avoidance, Evasion assistance control, Model predictive control

1 Introduction

There are almost 1.19 million road traffic deaths every year globally, where collision accidents account for about 98% [1, 2]. Intelligent vehicles, incorporating multi-source sensor systems and advanced control algorithms, have emerged as a promising solution to improve road safety [3, 4]. On this basis, collision avoidance (CA) algorithms have been widely studied and the corresponding technologies such as forward collision warning (FCW), automatic emergency braking (AEB), autonomous emergency steering (AES), etc. are used in ADAS in production vehicles [5–7].

Longitudinal CA system generates the desired deceleration through the braking system and avoids collision or reduces the degree of collision by lowering the vehicle's speed. The decision logic and control execution are relatively simple, which essentially controls the speed difference or distance difference between the ego vehicle (EV) and the obstacle vehicle (OV) [8]. Lateral CA system is to generate enough lateral displacement through the steering system to minimize the lateral overlap between the EV and the OV [9].

However, relying solely on longitudinal braking has inherent limitations in evasion. Ref. [10] evaluates AEB systems in six commercially available vehicles and shows

*Correspondence:
Zhuoren Li
1911055@tongji.edu.cn
[1] School of Automotive Studies, Tongji University, Shanghai 201804, China
[2] DIAS Automobile Electronics Co., Ltd., Shanghai 201206, China
[3] Department of Mechanical and Mechatronics Engineering, University of Waterloo, Waterloo, ON N2L 3G1, Canada

Springer Open

© The Author(s) 2025. **Open Access** This article is licensed under a Creative Commons Attribution 4.0 International License, which permits use, sharing, adaptation, distribution and reproduction in any medium or format, as long as you give appropriate credit to the original author(s) and the source, provide a link to the Creative Commons licence, and indicate if changes were made. The images or other third party material in this article are included in the article's Creative Commons licence, unless indicated otherwise in a credit line to the material. If material is not included in the article's Creative Commons licence and your intended use is not permitted by statutory regulation or exceeds the permitted use, you will need to obtain permission directly from the copyright holder. To view a copy of this licence, visit http://creativecommons.org/licenses/by/4.0/.

that they could only ensure successful CA at speeds below 50 km/h. From the study of Continental, it can be more intuitively found that the longitudinal CA system is usually able to safely avoid collisions at low relative speeds, while the lateral CA system is able to avoid crashes more efficiently at medium and high relative speeds [11]. Figure 1 schematically shows the relationship between the distance required for CA and the relative vehicle speed, including the distance of the last point to brake (LPTB) and the distance of the last point to steer (LPTS) [12]. As the relative speed increases, the LPTB distance gradually approaches and exceeds the LPTS distance. For conditions where the relative speed is above 45 km/h, it is easier to accomplish CA by using lateral CA methods.

Analysis of driver behavior in Ref. [11] indicates that as the urgency of CA intensifies, drivers involuntarily take more CA avoidance maneuvers by steering. However, lateral CA requires timely and appropriate steering maneuvers, placing significant demands on the driver's skills. Driver's underreaction or understeering can result in minor collisions with a low overlap rate, while the overreaction or oversteering may lead to vehicle instability or even critical safety accidents [13]. Consequently, it becomes crucial to provide steering assistance to drivers through evasion assistance control (EAC) to enhance driving safety during emergency CA.

Current EAC technologies can be divided into two types: (1) driver-activated EAC and (2) automatic EAC. Driver-activated EAC helps the driver adjust the vehicle motion according to the vehicle states by providing assisted steering torque after detecting the driver's steering intention [14]. Additionally, the driver's braking operation can also activate the EAC [15]. This approach ensures driver involvement when allocating control rights to the EAC controller and could reduce the risk of system misjudgment. Unlike the driver-activated EAC system, automatic EAC could predict the likelihood of a collision within a short period of time and intervene automatically to avoid collision [16]. This control method does not require driver activation and relieves the dependence on the driver's decision, which also improves the performance of CA. Ref. [17] designs a feedforward plus linear state feedback controller to enable the vehicle to track reference lateral acceleration through the booster torque of the EPS motor. Based on nonlinear backstepping control and adaptive sliding model control algorithms, Ref. [18] constructed integrated steering and braking controllers to implement emergency CA. In Ref. [19], the desired steering angle is determined based on the planned evasion assistance path, and a steering wheel assisted torque is then provided to fulfill the steering tracking requirement. However, automatic EAC is often difficult to consider the driver's intent, and may cause safety risks by interfering with the driver's reasonable steering maneuvers [20]. Consequently, a critical challenge lies in effectively combining the control outputs of the EAC controller and the driver.

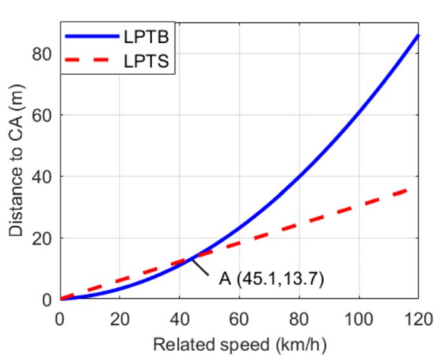

Figure 1 Schematic diagram of LPTB and LPTS

Several studies have been conducted to enhance the performance of shared control between automatic EAC systems and human drivers by incorporating various driver operational characteristics into the control algorithm design. Ref. [9] introduces an adaptive pre-targeting distance mechanism to develop an assisted steering torque controller that considers different drivers' driving styles. Using fuzzy control, Ref. [21] designs a dynamic distribution of driving authority to improve driver comfort. To address the conflict between humans and machines at the trajectory planning layer, Ref. [22] utilized potential-field-driven model predictive control to consider the driver-vehicle dynamics and the driver-related costs. The generated target trajectory represents a fusion of both the driver's input and the EAC system, potentially reducing conflicts between the EAC controller and the driver. However, due to the uncertainty of the driver's behavior, it is still challenging to coordinate driver preferences and EAC outputs at the trajectory planning level [23]. To improve the robustness of target path tracking, Ref. [24] optimizes the human-machine weights at the control layer, and utilizes the weighted input of driver's steering wheel torque as a disturbance to the controller. In order to integrate driving intention, driver operation, and vehicle driving state assessment, Ref. [25] designed a fuzzy weight assignment mechanism for human-machine coordination. Ref. [26] divided the driving space into safety and danger areas, and then evaluated the risk degree corresponding to the vehicle's position, which is used to determine the shared control weight. By considering driver state detection, human-machine conflict, and vehicle driving safety, Ref. [27] developed a more intricate weight assignment method.

However, these hierarchical weight assignment schemes consider the control system and the driver as independent operators and do not adequately account for the driver's response characteristics. Simply weighting the control output could affect the control performance or even destabilize the algorithm.

This paper proposes a Multi-mode Evasion Assistance Control (MEAC) Method based on the intelligent Distributed-drive Electric Vehicle (DDEV) platform. Leveraging the DDEV's capabilities of rapid, precise, and independent control over the four-wheel driving/braking torque response [28], this paper exploits the additional yaw moment as a control value to effectively address evasion assistance control, encompassing safety, stability, and comfort. Recognizing the variable nature of driver response and operation, this paper introduces a multi-mode EAC decision scheme for different emergency conditions. A reference safety area is established for EAC considering the safety and stability requirements, which serves as a guiding principle for evading obstacles. In particular, an integrated human-machine authority allocation mechanism is designed to mitigate conflicts between humans and machines during assistance control. The primary contributions are summarized as follows:

- A Multi-mode EAC framework is proposed to enhance CA performance. In shared mode, driver's steering maneuvers are properly corrected by the assisted steering wheel torque, which helps the driver to safely avoid a collision while keeping a feeling of control. In emergency mode, the steering angle is directly controlled along with the additional yaw moment to achieve emergency CA.
- A reference safety area for evasion assistance control is established, combining vehicle stability safety and road space safety. With the safety area, multi-objective model predictive control (MPC) problems considering collision safety, smoothness and reducing intervene are formed to solve the optimal control input for each EAC mode.
- An integrated human-machine authority allocation mechanism is designed, considering vehicle safety and the rationality of driver steering operations. The weight coefficients of the objective function are adapted according to behavioral safety and spatial safety, allowing the control intention of EAC to be adjusted in real-time.

The remainder of this paper is organized as: Section 2 introduces the whole system structure. In Section 3, the proposed MEAC method is described in detail. Section 4 is the specific implementation of the simulation and real vehicle experiment. Finally, Section 5 concludes this paper.

2 System Structure and Problem Statement

2.1 Problem Definition

In tests conducted by Bosch [29], Continental [12], Volvo [30] and many other research institutes or manufacturers, avoiding static obstacles in a straight line is considered as a typical lateral obstacle avoidance scenario. The goal of the proposed MEAC in this paper is to help the driver avoid collision in high-speed scenarios in the safest possible way through steering maneuvers. There are serval notations need to be defined to describe the CA problem.

Definition 1 The last point to braking (LPTB) refers to the start braking point where EV can just avoid collision by braking with the maximum deceleration. According to Ref. [31], the distance D_{LB} between the LPTB and the obstacle, as well as the corresponding Time-to-Collision TTC_{LB}, can be calculated as following:

$$\begin{cases} D_{LB} = (\tau_{eb} + \frac{\tau_{gb}}{2})v_r + \frac{(3.6v_r)^2}{25.92a_{bmax}}, \\ TTC_{LB} = D_{LB}/v_r \ , \end{cases} \tag{1}$$

where, τ_{eb} is the time to eliminate the braking clearance, τ_{gb} is the growth time of the braking force, v_r is the relative speed between EV and obstacle, and $a_{b\max}$ is the maximum braking deceleration.

Definition 2 The last point to steering (LPTS) refers to the start steering point on the original driving trajectory where the vehicle turns to the maximum extent just enough to avoid collision with obstacles. The distance D_{LS} between the LPTS and the obstacle, as well as the corresponding Time-to-Collision TTC_{LS}, can be calculated as follows:

$$\begin{cases} D_{LS} = \sqrt{\frac{2S_{offset}}{a_{lat}}}v_R, \\ TTC_{LS} = D_{LS}/v_R, \end{cases} \tag{2}$$

where, S_{offset} is the required lateral displacement for CA, and a_{lat} is the maximum lateral acceleration of the EV during CA [12].

Definition 3 When the perception sensor identifies a potential collision risk, the MEAC system will be activated after the TTC reaches a certain threshold, defined as the initial CA TTC_0.

The overall CA scenario is illustrated in Figure 2, where W_{EV} is the EV's width and W_{obs} is the width of obstacle, D_{obs} is the relative distance between EV and obstacle, d, d is the distance between EV and left, right road boundary respectively. d_{EAC} is lateral CA distance and d_{offset} is the

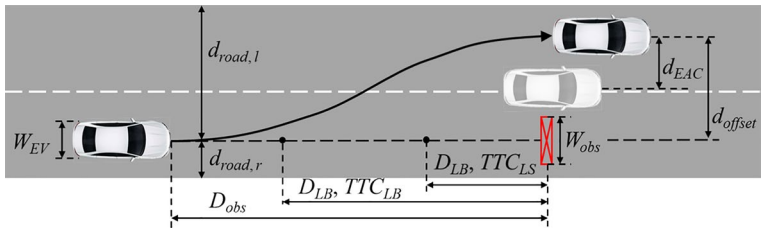

Figure 2 Collision avoidance scenario

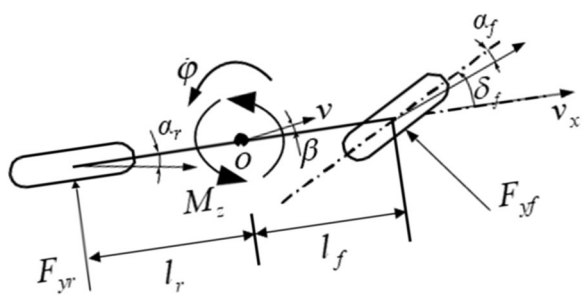

Figure 3 Two degree of freedom vehicle dynamics model

total lateral offset distance for CA. The EV can avoid the obstacle only when $d_{EAC} > 0$.

2.2 Vehicle System Model

In this paper, a two degree of freedom vehicle lateral dynamics model is used, as shown in Figure 3.

$$\begin{cases} \dot{\beta} = \frac{-2(C_{cf}+C_{cr})}{mv_x}\beta + \left(\frac{-2(C_{cf}l_f - C_e l_r)}{mv_x^2} - 1\right)\dot{\varphi} + \frac{2C_{bf}}{mv_x}\delta_f, \\ \ddot{\varphi} = \frac{-2(C_{cf}l_f - C_{cr}l_r)}{I_z}\beta + \frac{-2\left(C_{cf}l_f^2 + C_{cr}l_r^2\right)}{I_z v_x}\dot{\varphi} \\ \quad + \frac{2C_{cf}l_f}{I_z}\delta_f + \frac{M_z}{I_z}, \end{cases} \tag{3}$$

where I_z is the vehicle's yaw moment of inertia, m is the vehicle's mass, v_x is the vehicle's longitudinal speed, $\dot{\beta}$ is the sideslip angular velocity of the mass center, $\dot{\varphi}$ and $\ddot{\varphi}$ are the vehicle's yaw rate and yaw acceleration, respectively, l_f and l_r are the distance from the center of mass to the front axle and the rear axle, respectively, M_z is the direct yaw moment, δ_f is the steering angle of the front wheel, and C_{cf}, C_{cr} are the cornering stiffness of a single tire on the front and rear axles, respectively.

The components and forces of each part of the electric power steering system (EPS) are equivalent to the steering wheel and the upper section of the steering column, and the steering system model is established as Eq. (2):

$$J_e\ddot{\delta}_{sw} + B_e\dot{\delta}_{sw} = T_d + GT_m + T_{align} + T_f, \tag{4}$$

where $\dot{\delta}_{sw}$ and $\ddot{\delta}_{sw}$ are the steering angular velocity and angular acceleration of the upper section of the steering column, respectively. J_e and B_e are the equivalent moments of inertia and the equivalent damping of the steering system, respectively. T_d is the moment applied to the steering wheel by the driver. T_f is the equivalent friction torque, T_m is the torque at the output end of the steering power motor. G is the transmission ratio of the power-assisted motor reducer, and T_{align} is the aligning torque transmitted to the upper section of the steering column estimated by Ref. [32] as:

$$T_{align} = \frac{2C_{cf}L_p}{i_{steer}}\beta + \frac{2C_{cf}L_p}{i_{steer}}\frac{l_f\varphi}{v_x} - \frac{2C_{cf}L_p}{i_{steer}^2}\delta_{sw}, \tag{5}$$

where, L_p is the tire drag, and $i_{steer} = \delta_{sw}/\delta_f$ is the transmission ratio of the steering wheel angle and the front wheel angle.

2.3 EAC System Framework

This paper proposes the MEAC framework primarily designed for evasion scenarios at speeds of 45 km/h and above. The MEAC framework actively evaluates the vehicle's driving state, determining optimal timing and level of assistance control. Figure 4 illustrates the framework of the MEAC framework, which consists of four modules: (i) EAC mode decision, (ii) Safe area construction, (iii) Shared-EAC module (S-EAC), and (iv) Emergency-EAC module (E-EAC).

The safety of lateral CA mainly contains two aspects: one is the driving space safety, i.e., EV should not collide with obstacles or run out of the road boundary; the second is the driving state safety, i.e., EV could not lose its stability and then lead to the loss of control during lateral CA. Thus, the space safety area and the stability safety area are constructed as references and constraints for the EAC algorithm. The space safety area mainly considers driving space boundaries. The stability safety area is established based on the phase

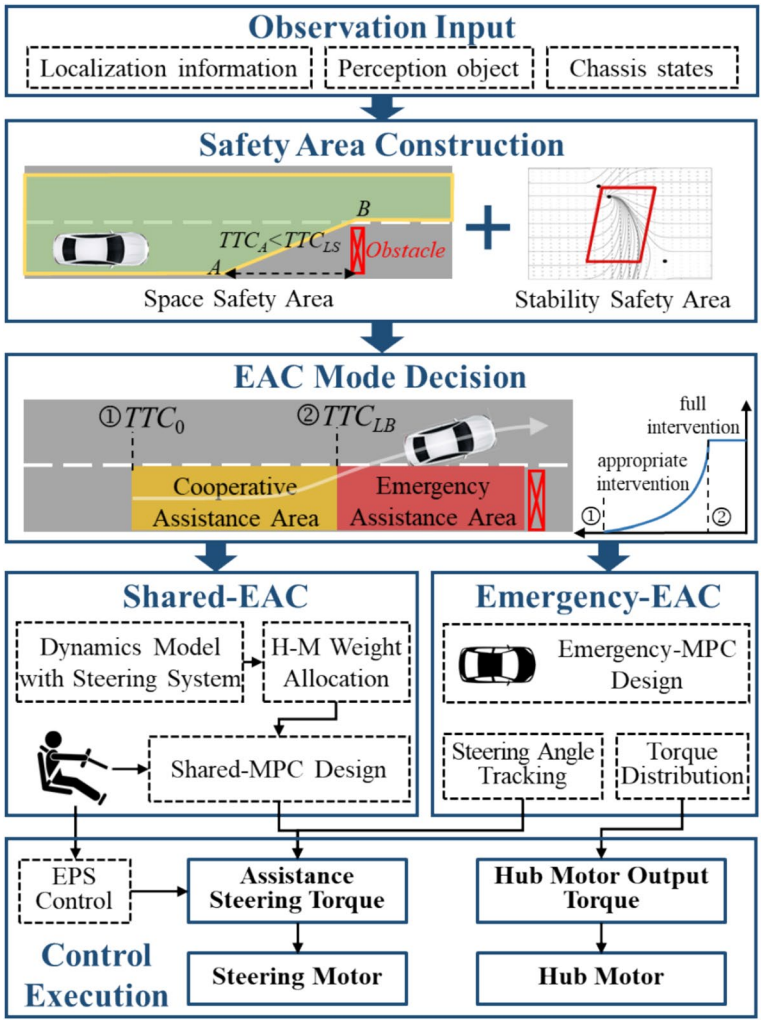

Figure 4 Schematic framework of the proposed MEAC

diagram of the sideslip angle and the yaw rate, referred to as the joint stability criterion [11].

Based on the vehicle's motion state and the surrounding environment features, the EAC mode decision module determines whether it is an assisted evasion situation or an emergency evasion situation. If the evasion urgency is low or the driver is already operating the vehicle, the MEAC system enters S-EAC mode to assist the driver in cooperative evasion. Conversely, if the urgency is high or the driver is not operating the vehicle to evade, it enters the E-EAC mode and the system takes direct control of the vehicle to execute emergency evasion. Specifically, some scenarios where collisions cannot be avoided are not in this paper's focus, such as obstacles that are too large for the E-EAC to still be able to accomplish evasion.

Finally, a multi-objective model MPC problem is formed for different EAC modes respectively. S-EAC integrates a human-machine authority allocation mechanism that includes space safety and driving behavior safety in the objective function design, which assists the driver in CA while reducing unnecessary intervention by the control system. For E-EAC, the control algorithm directly outputs the front wheel angle and additional yaw moment. These outputs are then executed by the lower-level angle tracking algorithm and motor torque distribution strategy.

3 Safety Area Construction and EAC Mode Decision

3.1 Space Safety Area

In the road coordinate system, the boundary of the space safety area consists of three parts: (1) the lane constraint boundary, restricting the maximum lateral displacement of EV, (2) the obstacle constraint boundary, which restricts the minimum lateral displacement of the vehicle,

(3) the vehicle kinematics constraint considering Ackerman steer characteristics. As illustrated in Figure 5(a), the left and right boundaries of the safety area are set by offsetting the outer lane boundary to the inside by a safe distance S_{safe}. Point A is the shape adjustment point of the lower boundary considering the vehicle steering characteristics. The corresponding predicted collision time TTC_A should be smaller than TTC_{LS} and $X_{sta} = D_{obs} - TTC_A v_r$. Additionally, a safety margin d_{safe} is allotted to the obstacle constraint boundary. Therefore, the upper and lower boundary of the space safety area ($Y_{\max}$ and $Y_{\min}$) can be designed as:

$$\begin{cases} Y_{\max}(X) = d_{road,l} - S_{safe}, \\ Y_{\min}(X) = \begin{cases} -d_{road,l} + S_{safe}, X < X_A, \\ \dfrac{(X - X_A)(\frac{W_{obs}}{2} + d_{safe} + d_{road,r})}{D_{obs} - X_A} - d_{road,r} + S_{safe}, X_A \le X < D_{obs}, \\ \dfrac{W_{obs}}{2} + S_{safe} + d_{safe}, X \ge D_{obs}. \end{cases} \end{cases} \tag{6}$$

The space safety coefficient was established based on the space safety domain, which is regarded as one of the reference foundations and evaluation metrics for EAC target setting and human-machine authority allocation. The space safety factor η_s is defined within a range of [0,1], with 0 indicating the highest level of danger and 1 indicating complete safety. As shown in Figure 5(b), the reference safety trajectory (X_{ref}, Y_{ref}) is divided into three segments considering the lateral movement during CA, which can be represented as follows:

$$\begin{cases} Y_{ref}(X_{ref}) = \begin{cases} 0, X_{ref} < X_{sta}, \\ \dfrac{X_{ref} - X_{sta}}{X_{obs} - X_{sta}} \cdot d_{offset}, X_{sta} \le X_{ref} < D_{obs}, \\ d_{offset}, X_{ref} \ge D_{obs}, \end{cases} \\ d_{offset} = \dfrac{Y_{\max}(D_{obs}) + Y_{\min}(D_{obs})}{2} = (\dfrac{W_{obs}}{2} + d_{safe} + d_{road,l})/2, \end{cases} \tag{7}$$

where (X_{sta}, 0) is the start steering point position. According the reference safety trajectory and the space safety area boundary, η_s can be expressed by Eq. (8):

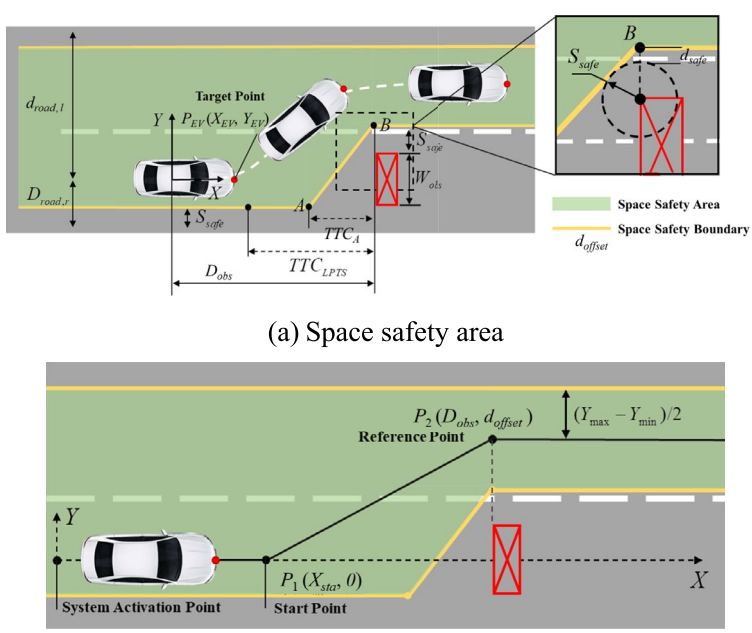

(a) Space safety area

(b) Reference safety trajectory

Figure 5 Schematic diagram of the space safety area and the reference safety trajectory

$$\eta_s = \begin{cases} 0,\ Y = Y_{safe}, \\ \dfrac{Y_{\max} - Y}{Y_{\max} - Y_{safe}}, Y_{safe} < Y < Y_{\max}, \\ \dfrac{Y - Y_{\min}}{Y_{safe} - Y_{\min}}, Y_{\min} < Y < Y_{safe}, \\ 1, Y \geq Y_{\max} \text{ or } Y \leq Y_{\min}. \end{cases} \tag{8}$$

It is worth noting that the reference safety trajectory is not the target trajectory tracked by the EAC. It is a judgment index for the authority allocation of human–machine control in the S-EAC. In addition, the reference safety trajectory can also "guide" the EV to a relatively safe position.

3.2 Stability Safety Area

During the emergency CA at high speed, the vehicle may be over-steered resulting in dangerous situations such as fishtailing or sideslip. In such cases, the vehicle's dynamic states may diverge and become unstable, causing the control system to fail.

In order to ensure the safety of lateral CA at the vehicle state level, it is necessary to analyze the vehicle dynamic characteristics and try to limit the dynamic states within the stability area. Based on Ref. [33], the vehicle stability safety area is designed based on the joint stability criterion of yaw rate and the sideslip angle, as shown in Figure 6. A closed parallelogram boundary is formed in the $\beta - \dot{\varphi}$ plane diagram as follows:

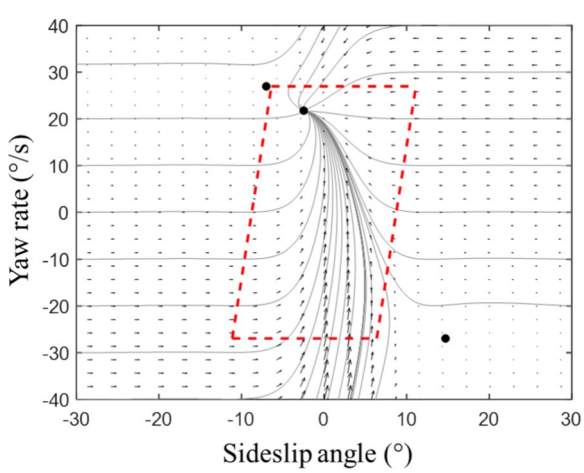

Figure 6 Schematic diagram of the stability safety area based on the $\beta - \dot{\varphi}$ plane with 60 km/h speed, 3° front steer angle and 0.8 road adhesion coefficient.

$$\begin{cases} \text{upper boundary: } \dot{\varphi}_{ss,\max} = \dfrac{\mu g}{v_x}, \\ \text{lower boundary: } \dot{\varphi}_{ss,min} = -\dfrac{\mu g}{v_x}, \end{cases} \tag{9}$$

$$\begin{cases} \text{left boundary: } \beta_{\min} = -\dfrac{1}{k_\beta}(\dot{\varphi} + \dfrac{\mu g}{v_x}) + \beta_{l,0}, \\ \text{right boundary: } \beta_{\max} = -\dfrac{1}{k_\beta}(\dot{\varphi} - \dfrac{\mu g}{v_x}) + \beta_{r,0}, \end{cases} \tag{10}$$

where, $\dot{\varphi}_{ss,\max}$, $\dot{\varphi}_{ss,\min}$ are the maximum and minimum steady-state yaw rate, respectively. v_x is the longitudinal speed, μ represents the road surface adhesion coefficient and g is the acceleration due to gravity. $\beta_{l,0}$ and $\beta_{r,0}$ are the sideslip angle at two saddle points.

3.3 EAC Mode Decision

The more urgent the lateral CA situation, the higher the demands on steering operations, and the greater the driver's reliance on the MEAC intervention. Figure 7 shows the relationship between the degree of intervention provided by the proposed MEAC and the timing of the driver's initiation of the steering operation (denoted as T_s). The work zone of MEAC is divided into two parts: the collaborative assistance area and the emergency assistance area, which determines whether the system goes into S-EAC mode or E-EAC mode.

The collaborative assistance area means the area before the EV reaches the LPTB, i.e., $TTC_0 > T_s > TTC_{LB}$. The driver can avoid collision via braking or steering. If the driver begins steering to avoid collisions, S-EAC is employed to appropriately assist or correct the driver's steering maneuvers with assisted steering wheel torque considering the operation intention of the driver. The S-EAC intervention time is equal to the time the driver starts to steer.

After the vehicle reaches the LPTB, i.e., $T_s < TTC_{LB}$, if the driver has not taken any CA actions, E-EAC directly controls the front wheel angle to avoid the collision via emergency lane changing. Additionally, the direct yaw

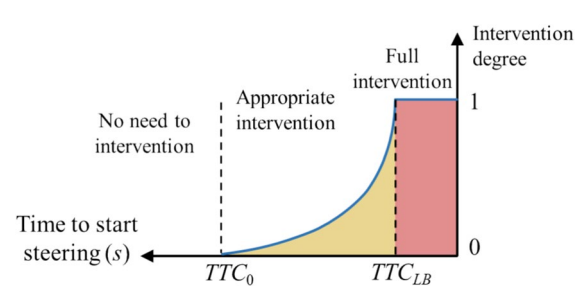

Figure 7 The intervention degree of MEAC

moment will be generated by the distributed-drive motors to improve the vehicle's stability.

4 Multi-mode Evasion Assistance Controller

4.1 Shared-EAC

1) System dynamics

After the vehicle reaches the LPTB, if the driver has not taken any CA actions, E-EAC directly controls the front wheel angle to avoid the collision via emergency lane changing. Additionally, the direct yaw moment will be generated by the distributed-drive motors to improve the vehicle's stability.

According to the system model built in Section 2.2, the state space is constructed as $\boldsymbol{\xi}_S = \left[\beta\ \dot{\varphi}\ \varphi\ Y\ \delta_{sw}\ \dot{\delta}_{sw}\right]^{\mathrm{T}}$. The control output is $\boldsymbol{\eta}_{C,S} = [\varphi\ \ Y]^{\mathrm{T}}$, and the constraint output is $\boldsymbol{\eta}_{B,S} = \left[\beta\ \dot{\varphi}\ Y\ \delta_{sw}\ \dot{\delta}_{sw}\right]^{\mathrm{T}}$. The control input is the equivalent assisted torque acting on the steering wheel, denoted as $u_S = T_{EAC}$. There is also the steering wheel torque T_d from the driver, which is regarded as a disturbance ω. The state-space equation of the continuous system is expressed in Eq. (11):

$$\begin{cases} \dot{\boldsymbol{\xi}}_S = \boldsymbol{A}_S\boldsymbol{\xi}_S + \boldsymbol{B}_S u_S + \boldsymbol{D}_S\omega, \\ \boldsymbol{\eta}_{C,S} = \boldsymbol{C}_{C,S}\boldsymbol{\xi}_S, \\ \boldsymbol{\eta}_{B,S} = \boldsymbol{C}_{B,S}\boldsymbol{\xi}_S, \end{cases} \tag{11}$$

where

$$\boldsymbol{A}_S = \begin{bmatrix} \frac{-2(C_{cf}+C_{cr})}{mv_x} & \frac{-2(C_{cf}l_f - C_{cr}l_r)}{mv_x^2} - 1 & 0 & 0 & 0 & 0 \\ \frac{-2(C_{cf}l_f - C_{cr}l_r)}{I_z} & \frac{-2(C_{cf}l_f^2 + C_{cr}l_r^2)}{I_z v_x} & 0 & 0 & 0 & 0 \\ 0 & 1 & 0 & 0 & 0 & 0 \\ v_x & v_x & 0 & 0 & 0 & 0 \\ 0 & 0 & 0 & 0 & 0 & 1 \\ \frac{2C_{cf}L_p}{i_{steer}J_e} & \frac{2C_{cf}l_f L_p}{i_{steer}J_e v_x} & 0 & 0 & \frac{-2C_{cf}L_p}{i_{steer}^2 J_e} & -\frac{B_e}{J_e} \end{bmatrix},$$

$$\boldsymbol{B}_S = \boldsymbol{D}_S = \left[0\ 0\ 0\ 0\ 0\ \frac{1}{J_e}\right]^{\mathrm{T}},$$

$$\boldsymbol{C}_{C,,S} = \begin{bmatrix} 0 & 0 & 1 & 0 & 0 & 0 \\ 0 & 0 & 0 & 1 & 0 & 0 \end{bmatrix},\ \boldsymbol{C}_{B,S} = \begin{bmatrix} 1 & 0 & 0 & 0 & 0 & 0 \\ 0 & 1 & 0 & 0 & 0 & 0 \\ 0 & 0 & 0 & 1 & 0 & 0 \\ 0 & 0 & 0 & 0 & 1 & 0 \\ 0 & 0 & 0 & 0 & 0 & 1 \end{bmatrix}.$$ The above continuous state-space equation is discretized by the forward Euler method and rewritten as:

$$\begin{cases} \tilde{\boldsymbol{\xi}}_S(k+1) = \tilde{\boldsymbol{A}}_{Sk}\tilde{\boldsymbol{\xi}}_S(k) + \tilde{\boldsymbol{B}}_{Sk}\Delta u_S(k), \\ \boldsymbol{\eta}_{C,S}(k) = \tilde{\boldsymbol{C}}_{C,Sk}\tilde{\boldsymbol{\xi}}_S(k), \\ \boldsymbol{\eta}_{B,S}(k) = \tilde{\boldsymbol{C}}_{B,Sk}\tilde{\boldsymbol{\xi}}_S(k), \end{cases} \tag{12}$$

In Eq. (12), $\tilde{\boldsymbol{\xi}}_S(k) = \left[\boldsymbol{\xi}_S(k)\ u_S(k-1)\ \omega(k-1)\right]^{\mathrm{T}}$, $\tilde{\boldsymbol{A}}_{Sk} = \begin{bmatrix} \boldsymbol{A}_{Sk} & \boldsymbol{B}_{Sk} & \boldsymbol{D}_{Sk} \\ \boldsymbol{0}_{1\times6} & \boldsymbol{I}_{1\times1} & \boldsymbol{0}_{1\times1} \\ \boldsymbol{0}_{1\times6} & \boldsymbol{0}_{1\times1} & \boldsymbol{0}_{1\times1} \end{bmatrix}$, $\tilde{\boldsymbol{C}}_{C,Sk} = \left[\boldsymbol{C}_{C,Sk}\ \boldsymbol{0}_{2\times1}\ \boldsymbol{0}_{2\times1}\right]$, $\tilde{\boldsymbol{C}}_{B,Sk} = \left[\boldsymbol{C}_{Sk}\ \boldsymbol{0}_{5\times1}\ \boldsymbol{0}_{5\times1}\right]$, $\boldsymbol{A}_{Sk} = T\boldsymbol{A}_S + \boldsymbol{I}$, $\boldsymbol{B}_{Sk} = T\boldsymbol{B}_S$, $\boldsymbol{D}_{Sk} = T\boldsymbol{D}_S$, $\boldsymbol{C}_{C,Sk} = \boldsymbol{C}_{C,S}$, $\boldsymbol{C}_{B,Sk} = \boldsymbol{C}_{B,S}$,

where T is the sampling time step, and $\boldsymbol{I}$ is an identity matrix whose dimension is the same as $\boldsymbol{A}_S$.

2) Objective function

The objective function of S-EAC is shown in following:

$$\min_{\boldsymbol{\Delta U}} J_S = \left\|\boldsymbol{H}_{C,S}(k) - \boldsymbol{H}_{Sref}(k)\right\|_{\boldsymbol{Q}_S}^2 + \left\|\boldsymbol{\Delta U}_S(k)\right\|_{\boldsymbol{R}_S}^2 + \left\|\Delta T_{EAC}(k) + T_{EAC}(k-1)\right\|_{\boldsymbol{N}_S}^2, \tag{13}$$

where $\boldsymbol{H}_{Sref}(k) = \left[\boldsymbol{\eta}_{C,Sref}(k+1)\quad \boldsymbol{\eta}_{C,Sref}(k+2)\quad \cdots\ \boldsymbol{\eta}_{C,Sref}(k+N_P)\right]^{\mathrm{T}}$ is the sequence of the reference control output $\boldsymbol{\eta}_{C,Sref}(k) = [\varphi_{offset}\ \ Y_{offset}]^{\mathrm{T}}$.

In the S-EAC mode, the control objectives include three items: (1) The vehicle's lateral displacement sequence and heading angle sequence should be close to the reference output sequence $\boldsymbol{H}_{Eref}(k)$. (2) The sum of control increment should be as small as possible to achieve smooth control. (3) $\Delta T_{EAC}(k)$ is the increment output of assisted torque by the S-EAC in each control cycle, and $T_{EAC}(k-1)$ is the assisted steering torque acting on the steering wheel in the last control cycle. Their sum is the assisted steering torque to be applied to the steering wheel in the current control cycle, which also should be small to reduce the intervention of the controller to the driver. $\boldsymbol{Q}_S$, $\boldsymbol{R}_S$, and $\boldsymbol{N}_S$ are the corresponding weight matrixes of each sub-objective. The relationship between $\Delta T_{EAC}(k)$ and $\Delta\boldsymbol{U}_S(k)$ is shown as:

$$\begin{cases} \Delta T_{EAS}(k) = \boldsymbol{\Delta U}_S(k)^{(1)} = \boldsymbol{S}_{\boldsymbol{U}_S}\boldsymbol{\Delta U}_S(k), \\ \boldsymbol{S}_{\boldsymbol{U}_S} = \left[1\ \boldsymbol{0}_{1\times(N_C-1)}\right]. \end{cases} \tag{14}$$

3) Constraints

Actuator constraints are set for the five output state sequences in the prediction horizon, which is shown as:

$$\begin{cases} \beta_{\min}(k) \le \beta(k) \le \beta_{\max}(k), \\ \dot{\varphi}_{\min}(k) \le \dot{\varphi}(k) \le \dot{\varphi}_{\max}(k), \\ Y_{\min}(k) \le Y(k) \le Y_{\max}(k), \\ \delta_{sw\ \min}(k) \le \delta_{sw}(k) \le \delta_{sw\ \max}(k), \\ \dot{\delta}_{sw\ \min}(k) \le \dot{\delta}_{sw}(k) \le \dot{\delta}_{sw\ \max}(k). \end{cases} \tag{15}$$

It is also necessary to constrain the control increment and control value to ensure that the required assisted wheel steering torque remains within the actuator's capacity, while preventing excessive assisted torque from interfering with driver operation or even injuring the driver.

$$\begin{cases} \boldsymbol{\Delta U}_{S\min} \le \boldsymbol{\Delta U}_S(k) \le \boldsymbol{\Delta U}_{S\max}, \\ \boldsymbol{U}_{S\min} \le \boldsymbol{U}_S(k) \le \boldsymbol{U}_{S\max}. \end{cases} \tag{16}$$

4) Human-machine control authority allocation

In order to reduce human-machine conflicts under S-EAC, this paper proposes a collaborative authority allocation mechanism, considering collision avoidance space safety factor η_s (proposed in Section 3.1) and the driving behavior safety factor η_d, which is calculated in real-time according to the η_s and the current driver's steering wheel torque output.

Defining the reference steering wheel torque for CA as:

$$\begin{cases} \text{if } Y \le Y_{\min}(D_{obs}),\ T_{ref} = \begin{cases} (1-\eta_s)T_{d,\max},\ Y \le Y_{ref}, \\ -(1-\eta_s)T_{d,\max},\ Y > Y_{ref}, \end{cases} \\ \text{if } Y > Y_{\min}(D_{obs}),\ T_{ref} = \begin{cases} -\mathrm{sgn}(\varphi)(1-\eta_s)T_{d,\max},\ Y \le Y_{ref}, \\ -(1-\eta_s)T_{d,\max},\ Y > Y_{ref}, \end{cases} \end{cases} \tag{17}$$

where, $T_{d,\max}$ is the driver's maximum steering wheel torque, $Y_{\min}(D_{obs})$ is the minimum required lateral distance to avoid collision, Y_{ref} is the reference lateral distance in Eq. (7). According to the relationship between the driver steering wheel torque T_d and the reference torque T_{ref}, η_d is defined as:

$$\eta_d = \begin{cases} 0,\ T_d \cdot T_{ref} < 0, \\ 1,\ T_d < T_{ref} < 0 \text{ or } T_d > T_{ref} > 0, \\ \dfrac{T_d}{T_{ref}},\ \text{else}. \end{cases} \tag{18}$$

It means if T_d and T_{ref} are in opposite directions, it is judged that the driver's steering behavior is unreasonable and driving behavior safety factor η_d is 0; if T_d and T_{ref} are in the same direction and the former is not smaller than the latter, the driver outputs sufficient steering wheel torque and η_d is 1. η_s and η_d jointly characterize the safety of the driver's CA maneuvers. Consequently, in the objective function in Eq. (13), the larger weight N_S assigned to the term that reduces the assisted torque, the more S-EAC tends to decrease its control weight and reduce its output, thereby minimizing unnecessary intervention with the driver when the operation is correct and the position is safe. Conversely, the smaller weight N, the more S-EAC tends to increase its control weight and prioritize CA by outputting assisted steering wheel torque, thereby helping the driver correct erroneous steering operations in dangerous situations. The weight N can be specifically calculated as follows:

$$\begin{cases} N_S = 1 \times 10^{(4\cdot\eta_N - 1)}, \\ \eta_N = \varepsilon(\eta_s \cdot \eta_d - 0.25) \cdot \eta_s \cdot \eta_d, \end{cases} \tag{19}$$

where $\varepsilon(\cdot) = 0$ or 1, is a step function, and η_s is the space safety factor from Eq. (8).

The solved assisted torque work together with the steering torque output from the EPS to the steering motor for cooperative evasion.

4.2 Emergency-EAC

1) Emergency MPC

In E-EAS mode, the MPC controller calculates the required front wheel angle and the additional yaw moment. Compared with the S-EAC control algorithm. The system state variables are set as $\boldsymbol{\xi}_E = [\beta\ \dot{\varphi}\ \varphi\ Y]^{\mathrm{T}}$, the control input is set as $\boldsymbol{u}_E = [\,\delta_f\ M_z\,]^{\mathrm{T}}$, the control output is set as $\boldsymbol{\eta}_{C,E} = [\,\varphi\ Y\,]^{\mathrm{T}}$, and the constraint output is set as $\boldsymbol{\eta}_{B,E} = [\,\beta\ \dot{\varphi}\ Y\,]^{\mathrm{T}}$.

The state equation is established as follows:

$$\begin{cases} \dot{\boldsymbol{\xi}}_E = \boldsymbol{A}_E\boldsymbol{\xi}_E + \boldsymbol{B}_E\boldsymbol{u}_E, \\ \boldsymbol{\eta}_{C,E} = \boldsymbol{C}_{C,E}\boldsymbol{\xi}_E, \\ \boldsymbol{\eta}_{B,E} = \boldsymbol{C}_{B,E}\boldsymbol{\xi}_E, \end{cases} \tag{20}$$

$$\boldsymbol{A}_E = \begin{bmatrix} \frac{-2(C_{cf}+C_{cr})}{mv_x} & \frac{-2(C_{cf}l_f - C_{cr}l_r)}{mv_x^2} - 1 & 0 & 0 \\ \frac{-2(C_{cf}l_f - C_{cr}l_r)}{I_z} & \frac{-2(C_{cf}l_f^2 + C_{cr}l_r^2)}{I_z v_x} & 0 & 0 \\ 0 & 1 & 0 & 0 \\ v_x & v_x & 0 & 0 \end{bmatrix},$$

$$\boldsymbol{B}_E = \begin{bmatrix} \frac{2C_{cf}}{mv_x} & 0 \\ \frac{2C_{cf}l_f}{I_z} & \frac{1}{I_z} \\ 0 & 0 \\ 0 & 0 \end{bmatrix}, \boldsymbol{C}_{C,E} = \begin{bmatrix} 0 & 0 & 1 & 0 \\ 0 & 0 & 0 & 1 \end{bmatrix}, \boldsymbol{C}_{B,E} = \begin{bmatrix} 1 & 0 & 0 & 0 \\ 0 & 1 & 0 & 0 \\ 0 & 0 & 0 & 1 \end{bmatrix}.$$

The control increment model is obtained by discretizing and expanding the system dynamics,

$$\begin{cases} \tilde{\boldsymbol{\xi}}_E(k+1) = \tilde{\boldsymbol{A}}_{Ek}\tilde{\boldsymbol{\xi}}_E(k) + \tilde{\boldsymbol{B}}_{Ek}\boldsymbol{\Delta u}_E(k), \\ \boldsymbol{\eta}_{C,E}(k) = \tilde{\boldsymbol{C}}_{C,Ek}\tilde{\boldsymbol{\xi}}_E(k), \\ \boldsymbol{\eta}_{B,E}(k) = \tilde{\boldsymbol{C}}_{B,Ek}\tilde{\boldsymbol{\xi}}_E(k), \end{cases} \tag{21}$$

$$\tilde{\boldsymbol{\xi}}_E(k) = \left[\, \boldsymbol{\xi}_E(k) \;\; u_E(k-1) \,\right]^{\mathrm{T}},\ \tilde{\boldsymbol{A}}_{Ek} = \begin{bmatrix} \boldsymbol{A}_{Ek} & \boldsymbol{B}_{Ek} \\ \boldsymbol{0}_{1\times 4} & \boldsymbol{I}_{1\times 2} \end{bmatrix},\ \tilde{\boldsymbol{B}}_{Ek} = \begin{bmatrix} \boldsymbol{B}_{Ek} \\ \boldsymbol{I}_{1\times 2} \end{bmatrix},$$

$$\tilde{\boldsymbol{C}}_{C,Ek} = \left[\, \boldsymbol{C}_{C,Ek} \;\; \boldsymbol{0}_{2\times 1} \,\right],\ \tilde{\boldsymbol{C}}_{B,Ek} = \left[\, \boldsymbol{C}_{B,Ek} \;\; \boldsymbol{0}_{3\times 1} \,\right].$$

The objective function of the E-EAC mode is designed as

$$\begin{aligned} &\min_{\boldsymbol{\Delta U}_E} J(\tilde{\boldsymbol{\xi}}_E(k), \boldsymbol{\Delta U}_E(k)) \\ &= \left\| \mathbf{H}_{C,E}(k) - \mathbf{H}_{Eref}(k) \right\|_{\boldsymbol{Q}_E}^2 + \left\| \boldsymbol{\Delta U}_E(k) \right\|_{\boldsymbol{R}_E}^2, \end{aligned} \tag{22}$$

where $\boldsymbol{H}_{C,E}(k)$ and $\boldsymbol{H}_{Eref}(k)$ are taken in a similar way to S-EAC, and $\boldsymbol{Q}_E$, and $\boldsymbol{R}_E$ are the corresponding weight matrixes. The constraint setting of the control increment, control input, and control output in E-EAC are same with those in S-EAC.

Table 1 Parameters of different driver model

Driver model	τ_d (ms)	k_c(Nm/rad)	k_b(Nm·s/rad)	k_L	k_A
Underreaction	300	50	0.7	10	40
Overreaction	150	150	1.2	70	100

5 Simulation and Experimental Test

5.1 Parameter Setting

For the MEAC algorithm, $T = 0.05$ s, N_p=20 and N_c=10, $\boldsymbol{Q}_S = \mathrm{diag}\{3\times10^3,\ 2\times10^2\}$, $\boldsymbol{R}_S = 10^2$, $\boldsymbol{Q}_E = \mathrm{diag}\{4\times10^3,\ 2\times10^2\}$, $\boldsymbol{R}_E = 2\times10^4$. According to Ref. [34], two driver models including underreaction and overreaction are constructed by setting the driver reaction delay time τ_d, the driver's muscle stiffness coefficient k_c and the driver's muscle damping coefficient k_b. k_L and k_A are the parameters for the driver tracking algorithm (more details in Ref. [34]). The parameter settings for driver model in this paper are shown in Table 1. The proposed EMAC is implemented with two driver models in S-EAC, and the comparison baseline is the driver model only with EPS assistance [35]. For E-EAC, the comparison baseline is the MPC algorithm without with additional yaw moment control [11].

5.2 Simulation Results

IPG CarMaker and MATLAB/Simulink are applied to build a joint simulation platform, as shown in Figure 8.

The simulation scenario is a straight two-lane structured road. The one side lane width is 3.5 m, and the road adhesion coefficient μ is 0.8. The target speed is 60 km/h and EV maintain this speed during CA. According to Ref. [34], the initial CA TTC_0 is set to 2.5 s, the obstacle will also suddenly appear in front of the vehicle at this time

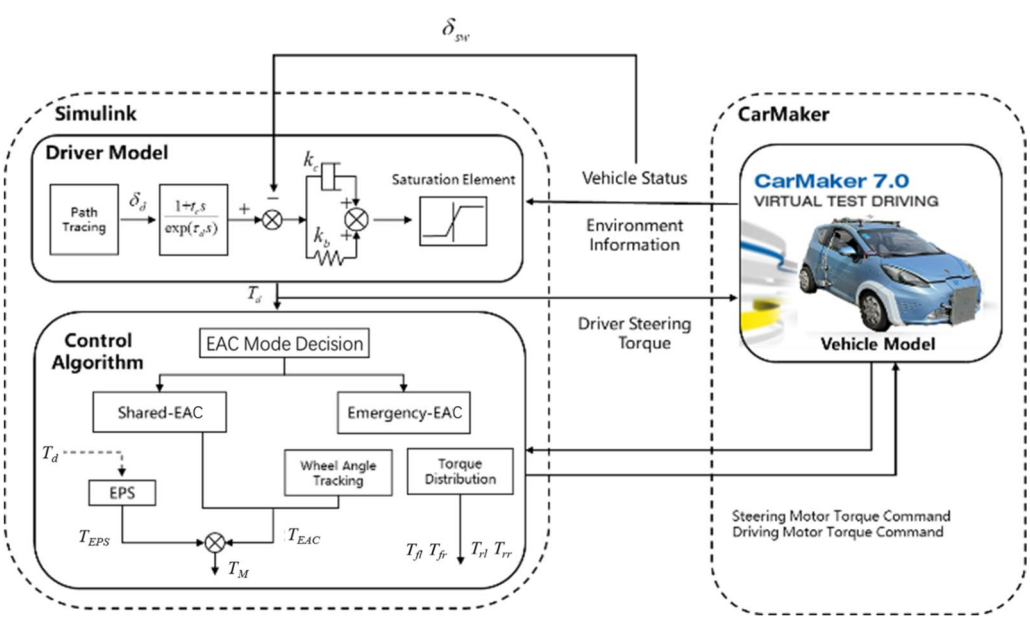

Figure 8 CarMaker-MATLAB/Simulink joint simulation platform with different driver model

with D_{obs} =100 m, and the width of the obstacle W_{obs} is 1.9 m.

5.2.1 S-EAC Simulation

In the simulation test of S-EAC, the driver begins steering to avoid a collision at T_s =2 s.

1) Underreaction scenario

The CA trajectories in this scenario are shown in Figure 9. Due to insufficient steering by the underreaction driver, the vehicle's lateral displacement during CA maneuvers is inadequate, resulting in a collision with the obstacle. With the assisted steering wheel torque of S-EAC, EV rapidly increases the lateral displacement and eventually avoids the collision. As shown in Figure 10(a) and (b), the driver's underreaction for CA results in a lower output steering wheel torque. It can be seen that the assisted steering wheel torque is applied to help the driver increase steering at $t = 1.2$ s ($X = 73.8$ m), and then to aid in returning steering at $t = 2.3$ s ($X = 92$ m). Therefore, the steering wheel angle of S-EAC is significantly higher than baseline during 1.34 and 3.2 s in Figure 10(c), which results in a higher Space safety factor for CA. In this scenario, the longitudinal distance traveled by the EV with S-EAC to achieve the required lateral displacement for CA is reduced from 49 to 36.8 m, representing a 24.8% reduction compared to the baseline. Theses results proof that proposed S-EAC can enhance CA safety in the case of driver underreaction.

2) Overreaction scenario

Similar to the underreaction scenario, the CA trajectories and the corresponding quantitative results are shown in Figures 11 and 12. Without S-EAC, the vehicle eventually run out of the lane boundary due to the driver's excessive steering maneuver that is not corrected in time. While the S-EAC corrected the oversteering maneuver in time and keep the vehicle within the lane boundary to CA. The driver's overreaction leads to a large steering torque at the initial stage of CA. The assisted steering wheel torque by S-EAC does not output before t=1.8 s because the MEAC system believes that the vehicle can safely avoid the collision under the driver's current control. As the driver continues to apply a large steering wheel angle without returning in time, the control system assesses that collision avoidance is dangerous, and thus it outputs a reverse assisted torque to help the driver adjust steering until the vehicle avoids the obstacle. With the assisted steering wheel torque by S-EAC, the vehicle returns itself early and the lateral displacement increasing is suppressed. The maximum lateral displacement is reduced from 5.43 to 3.69 m, reducing 32% compared to baseline.

5.2.2 E-EAC Simulation

In the simulation test of emergency CA where there is no CA operation by the driver and thus the E-EAC is active at $T_s = TTC_{LB} = 1.38$ s.

From Figure 13, it can be seen that both two methods safely accomplish the emergency CA task. At the beginning of CA, the additional yaw moment enhances the change rate of the lateral displacement to better avoid obstacle. As shown in Figure 14(a), the maximum steering wheel angle of E-EAC is reduced from 83.6° to 79.2° during the left-turn to CA, and reduced from 83.5°

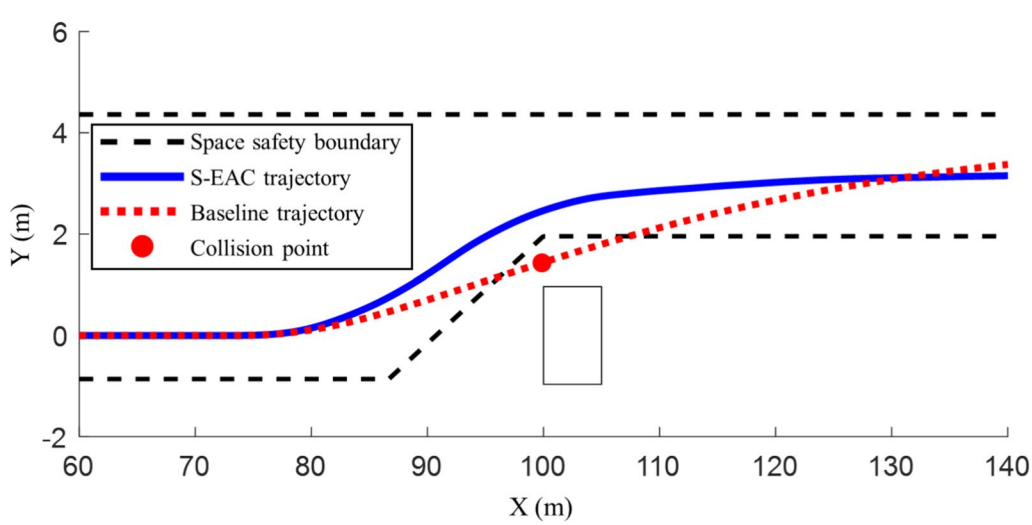

Figure 9 CA trajectory with underreaction driver model

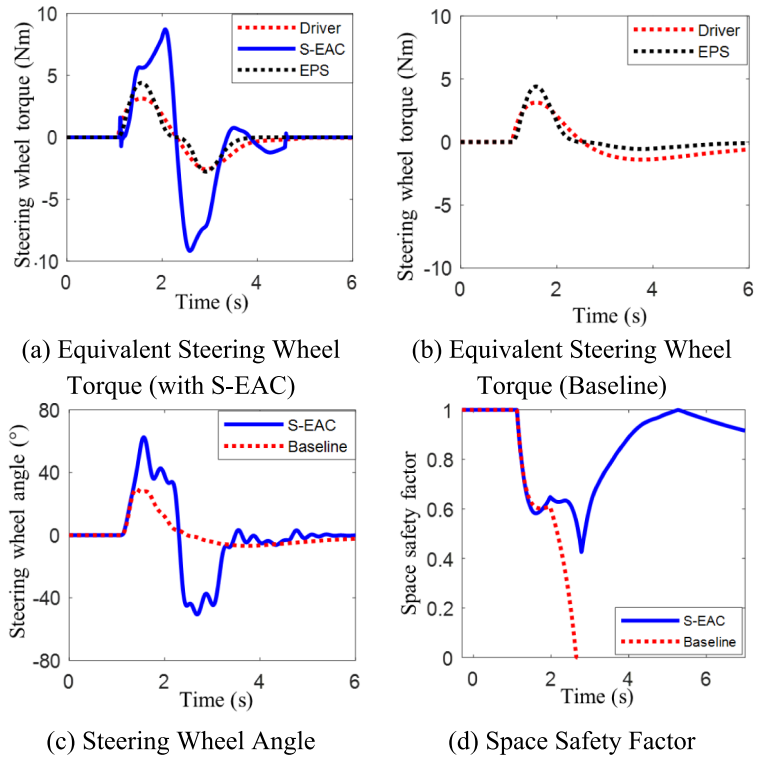

Figure 10 Simulation results of S-EAC with underreaction driver model

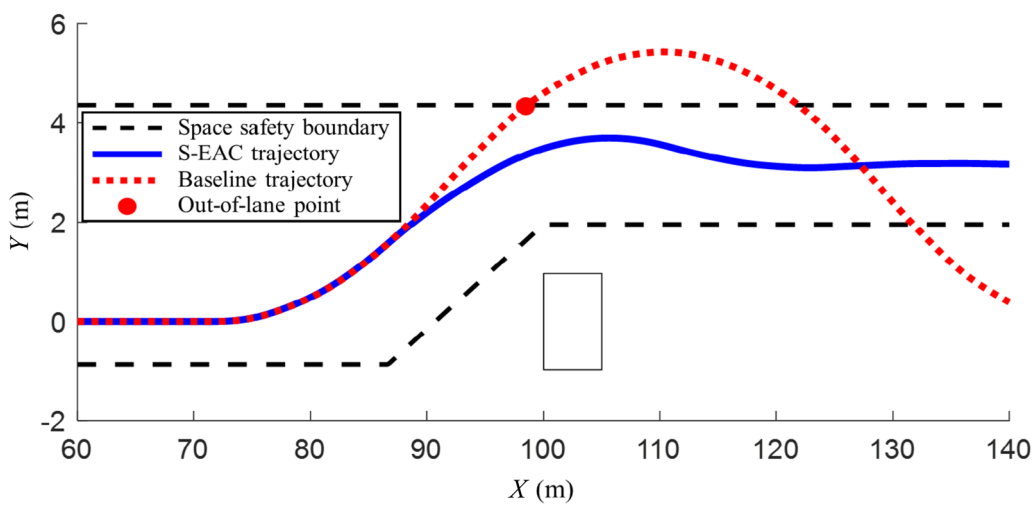

Figure 11 CA trajectory with overreaction driver model in simulation

to 71.5° during the return. This steering wheel angle amplitude is reduced while ensuring safe CA. Moreover, the steering wheel angle with E-EAC returns more quickly, making the vehicle correct the heading more quickly and reduces the lateral displacement overshoot. The maximum lateral displacement of E-EAC is 3.16 m, which does not produce an overshoot, while 3.53 m of baseline, whose overshoot reaches 10.6%. As shown in

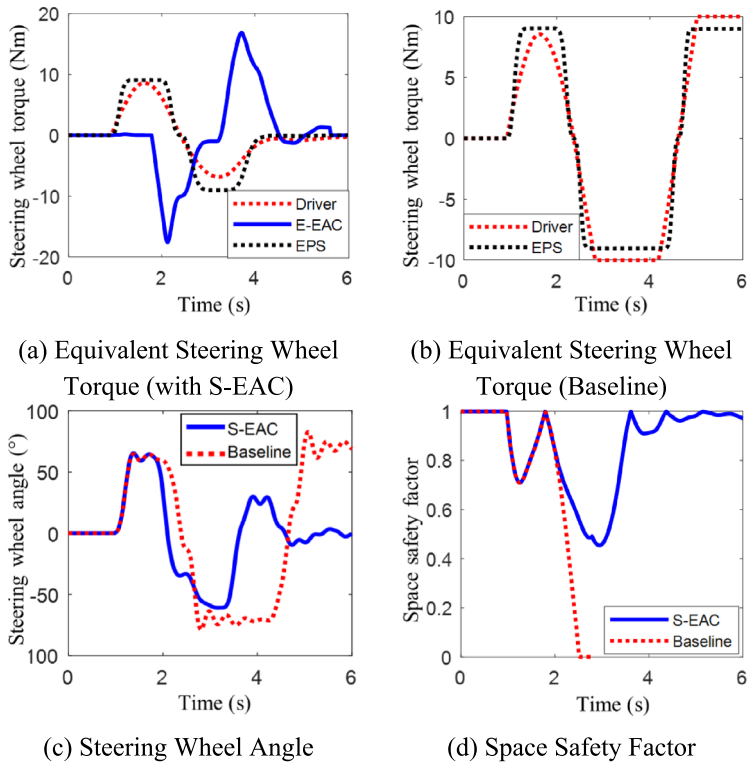

(a) Equivalent Steering Wheel Torque (with S-EAC)

(b) Equivalent Steering Wheel Torque (Baseline)

(c) Steering Wheel Angle

(d) Space Safety Factor

Figure 12 Simulation results of S-EAC with overreaction driver model

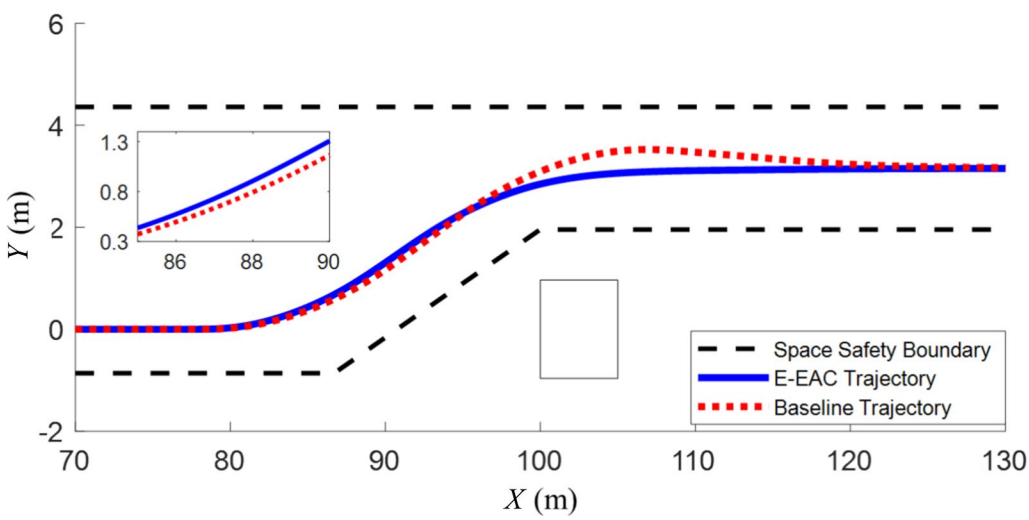

Figure 13 Emergency CA trajectory in simulation

Figure 14(d), the lowest space safety factor of E-EAC is 0.71, while that of the baseline is 0.57, increased by 24%. The simulation results show that the E-EAC algorithm can improve the efficiency and safety of lateral CA.

5.3 Real Vehicle Test

To further test our approach, we conducted real-vehicle tests with an intelligent vehicle test platform with four-wheel motors, as shown in Figure 15. The localization is provided by a GJ high-precision differential localization device. The torque, speed, and other signals

of the driving motor and steering wheel torque sensor signals are obtained through the vehicle management system. The proposed MEAC algorithm runs on the Flexbench vehicle controller from AUDESSE. The output control command signal from vehicle controller is sent to the chassis to control the vehicle via CANBus

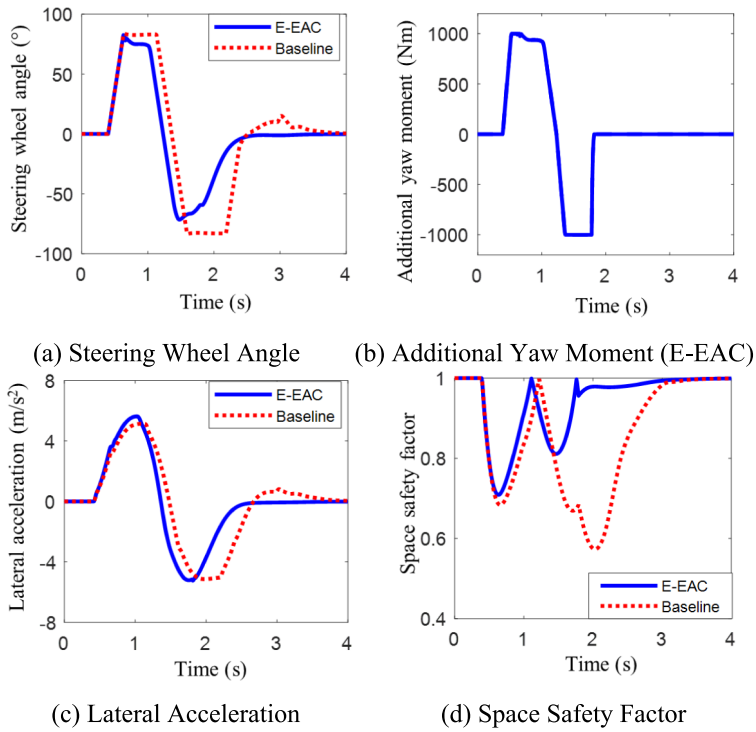

Figure 14 Simulation results of E-EAC

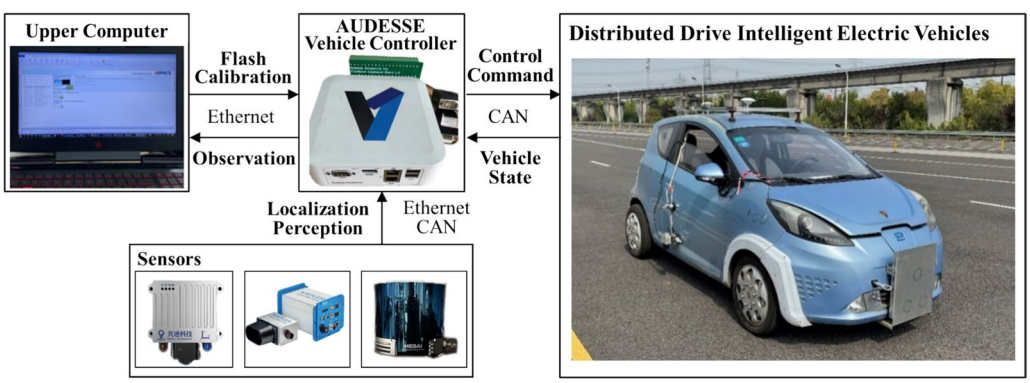

Figure 15 Real vehicle test platform

Table 2 Parameters of the real test vehicle

Parameters	Values	Parameters	Values
Mass (kg)	1360	Height of center-of-mass (m)	0.54
Wheelbase (m)	2.305	Distance between front-axle to center-of-mass (m)	1.112
Yaw Moment Inertia (kg m^2)	1785	Distance between rear-axle to center-of-mass (m)	1.193
Gear ratio	16.68	Wheel radius (m)	0.29

communication. Table 2 shows the relevant parameters of the test vehicle, and the speed in real vehicle test is 45 km/h.

5.3.1 S-EAC Real Vehicle Test

1) Underreaction scenario

During the underreaction test, the driver lightly touches the steering wheel to demonstrate low muscle tension and uses a lower steering frequency and amplitude to simulate the driver's inadequate steering.

As shown in Figure 16, the vehicle without S-EAC nearly collided with the obstacle. Upon activation of S-EAC at $t = 0.74$ s, the system promptly increases the vehicle's lateral displacement and corrects the heading angle to maintain safe lateral movement. The

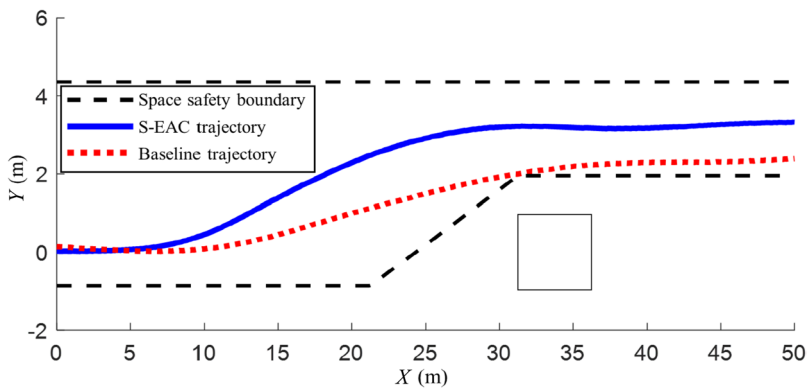

Figure 16 CA trajectory with underreaction driver in real vehicle test

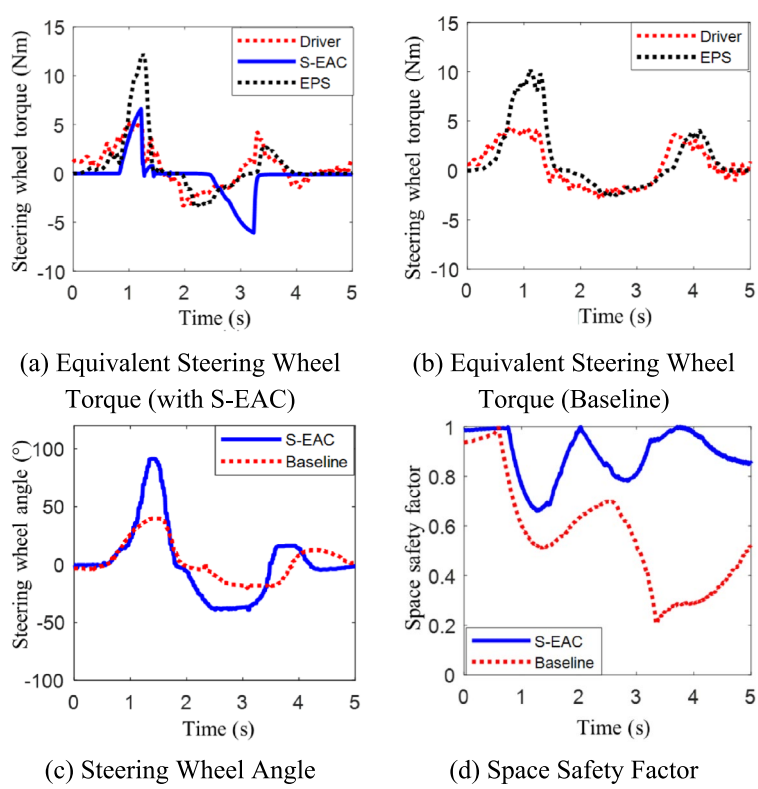

Figure 17 Real vehicle test results of S-EAC with underreaction driver model

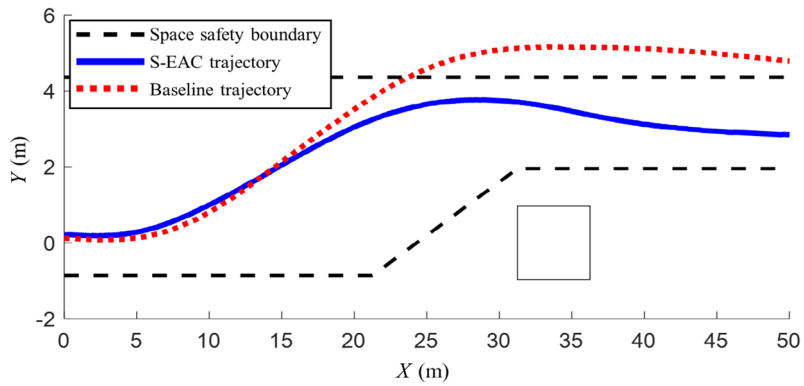

Figure 18 CA trajectory with overreaction driver in real vehicle test

longitudinal displacement needed to achieve the minimum lateral safety distance decreases from 31.25 to 18.04 m, by 42.27% reduction compared to baseline. Figures 16(b) and 17(a) shows the equivalent steering wheel torque of two methods. The assisted torques are applied between 0.82–1.45 s and 2.45–3.32 s, aiding the driver in steering. Thus, the steering wheel angle of S-EAC is larger than baseline between 1.07–1.69 s and 2.4–3.4 s, as shown in Figure 17(c), directly reflecting the impact of the assisted torque on the vehicle's lateral motion. The space safety factor in Figure 17(d) indicates that the minimum space safety factor during CA increases from 0.21 to 0.66 with the use of evasion assistance control.

Test results demonstrate that the S-EAC can increase steering amplitude to improve CA safety when the driver's steering operation is inadequate.

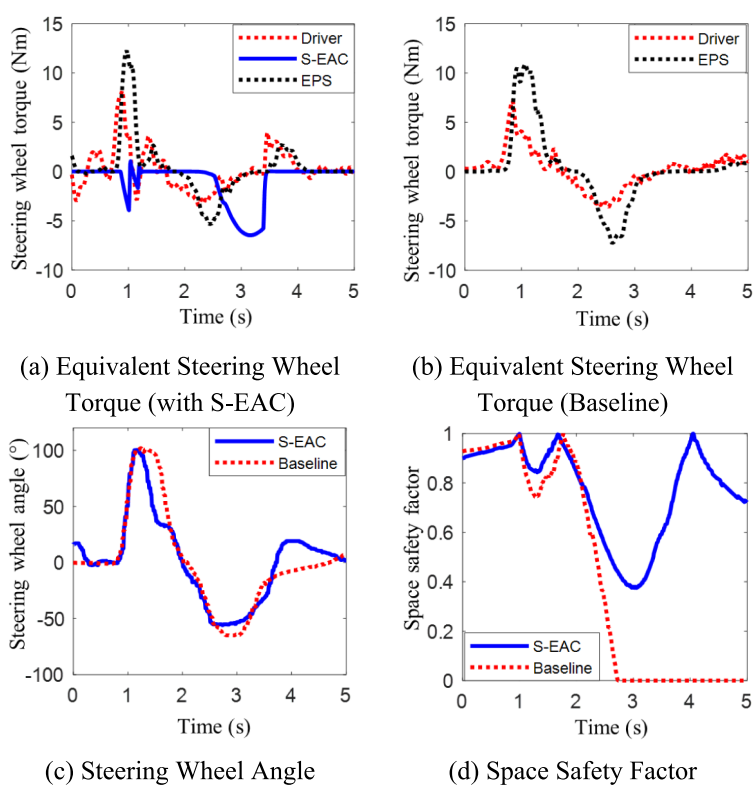

Figure 19 Real vehicle test results of S-EAC with underreaction driver model

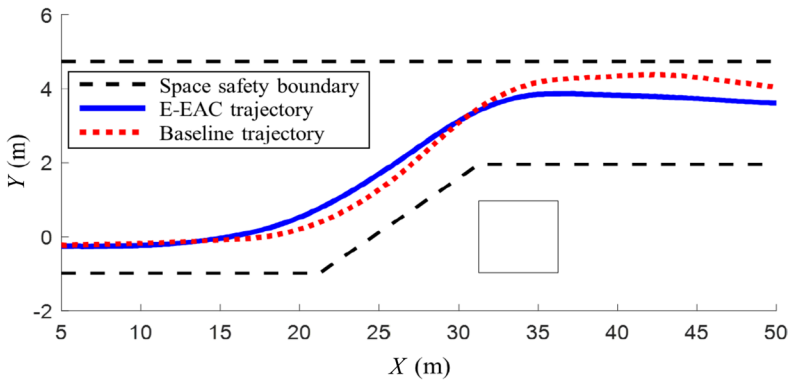

Figure 20 Emergency CA trajectory in real vehicle test

3) Overreaction scenario

To simulate the overreaction driving conditions leading to oversteering, the driver holds the steering wheel tightly with high muscle tension, steers quickly with a large steering wheel torque, and returns slowly during the CA progress.

Figure 18 is the CA trajectory of two methods with overreaction driver. Without S-EAC, the vehicle's excessive steering resulted in excessive lateral displacement, surpassing the space safety boundary. With S-EAC, the controller promptly adjusts the steering wheel angle to mitigate the excessive lateral displacement. Consequently, the vehicle's maximum lateral displacement is reduced from 5.76 to 3.76 m, a decrease of 34.7%. In Figure 19(a), S-EAC outputs assisted torque between 0.87–1.21 s and 2.40–3.46 s, both correcting the steering to the right. The corresponding steering wheel angle in Figure 19(c) returns earlier compared to the baseline. As shown in Figure 19(d), the space safety factor of baseline becomes 0 at 2.73 s after the vehicle crossing the space boundary. With S-EAC, the minimum space safety factor increases to 0.38 and the average space safety factor is improved to 0.75, which confirm the effectiveness of S-EAC in correcting driver steering maneuvers with oversteer operation.

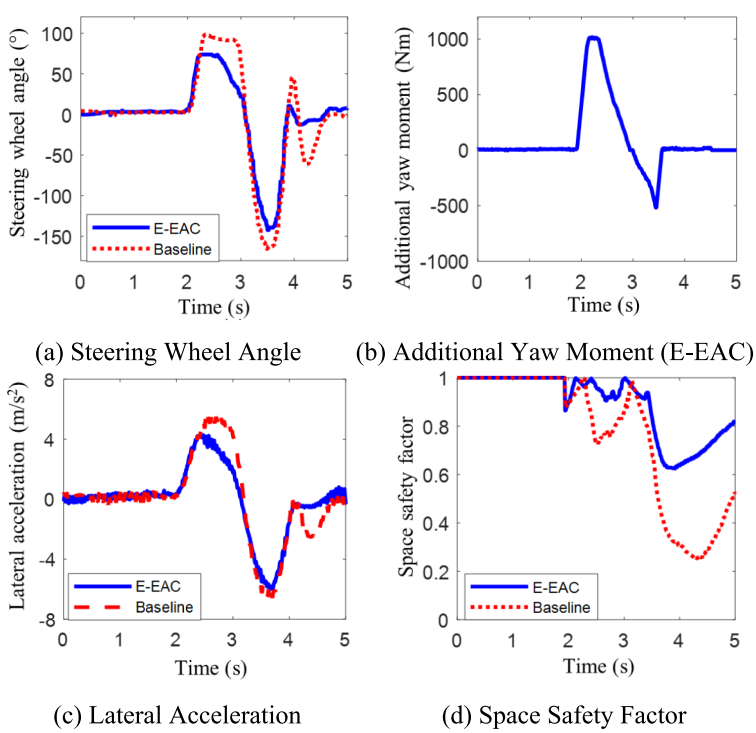

Figure 21 Real vehicle test results of E-EAC with underreaction driver model

5.3.2 E-EAC Real Vehicle Test

Figures 20 and 21 are the results of the E-EAC real vehicle test. With additional yaw moment control, the change rate in lateral displacement for CA is enhanced without increasing the steering wheel angle. It also corrects the heading more quickly, reducing overshoot of lateral displacement compared to the baseline. The longitudinal distance of E-EAC traveled to reach the minimum lateral displacement for CA is 8.30 m, reduced by 12.2% compared to the 9.45 m of baseline. E-EAC also reduced the lateral overshoot relative to the reference trajectory by 50.1% and the maximum lateral acceleration by 9.8%. For the baseline, the minimum space safety factor is 0.252, with an average space safety factor of 0.6593. In contrast, the minimum space safety factor of E-EAC increased to 0.626, and the average space safety factor improved to 0.8376. These results demonstrate the effectiveness and safety of E-EAC for emergency CA.

6 Conclusions

This paper proposes a multi-mode evasion assistance control (MEAC) framework for intelligent distributed-drive electric vehicles (DDEV) that effectively reduces human-machine conflicts and enhances collision avoidance safety performance. It considers the dynamic nature of the human driver's steering response and intervenes to correct the driver's actions when their collision avoidance operation is deemed inappropriate. The space safety area and stability safety area are constructed to provide reference and constraints for evasion control in different modes. In the Shared-EAC mode (S-EAC), a human-machine authority allocation mechanism is designed to solve the optimal control sequence based on model predictive control. In cases where the human driver is unable to avoid a collision, the emergency EAC (E-EAC) can perform emergency collision avoidance control with additional yaw moment. Simulation and experimental tests are conducted to validate the effectiveness of the proposed MEAC. It successfully performs collision avoidance assistance maneuvers with different driver models, showcasing outstanding human-machine coordination and ensuring safe collision avoidance. In future work, the analysis and understanding of driver intent and the complex dynamic scenario will be further enhanced to provide more stable and reliable cooperative assistance control.

Acknowledgements
Not applicable.

Author contributions
BL, ZL, CY developed the idea for the study; BL, ZL, CY were in charge of the whole trial; BL, ZL wrote the manuscript; YL, AK, LX revised the manuscript. All authors read and approved the final manuscript

Funding
Supported by National Key Research and Development Program of China (Grant Nos. 2022YFE0117100 and 2021YFB250120101), National Natural Science Foundation of China (Grant No. 52325212), Shanghai Municipal Automotive Industry Science, Technology Development Foundation (Grant No. 2203) and the SAIC Motor Corporation Limited (Grant No. 2023023).

Data Availability
The datasets used and/or analysed during the current study are available from the corresponding author on reasonable request.

Declarations

Competing Interests
The authors declare that they have no competing interests.

Received: 8 September 2024 Revised: 8 May 2025 Accepted: 19 May 2025
Published online: 20 June 2025

References

[1] World Health Organization. *Global Status Report on Road Safety 2023*. Geneva, Switzerland: World Health Organization, 2023.
[2] National Highway Traffic Safety Administration. *Traffic safety facts 2022*. US Dept. Transp., 2023. 711–790.
[3] C Tian, C Huang, Y Wang, et al. Recent estimation techniques of vehicle-road-pedestrian states for traffic safety: Comprehensive review and future perspectives. *IEEE Transactions on Intelligent Transportation Systems*, 2025, 26(3): 2897–2920.
[4] Z Zhang, G Yin, C Huang, et al. Fuzzy adaptive state estimation of distributed drive electric vehicles with random missing measurements and unknown process noise. *Chinese Journal of Mechanical Engineering*, 2024, 37: 118.
[5] C X Sun, Y T Li, H Y Li, et al. Forward collision warning strategy based on millimeter-wave radar and visual fusion. *Sensors*, 2023, 23(23): 9295.
[6] J B Cicchino. Effects of forward collision warning and automatic emergency braking on rear-end crashes involving pickup trucks. *Traffic Inj. Prev.*, 2023, 24(4): 293-298.
[7] H D Nguyen, D Kim, Y S Son, et al. Linear time-varying MPC-based autonomous emergency steering control for collision avoidance. *IEEE Transactions on Vehicular Technology*, 2023, 72(10): 12713-12727.
[8] X J Zhang, S Li, K H Guo, et al. Efficient cooperative adaptive cruise control including platoon kinematics. *Automotive Innovation*, 2024, 7: 271–282.
[9] C Ge, J B Zhang, H B Yao, et al. Trajectory planning for autonomous vehicle with numerical optimization method. *Automotive Innovation*, 2024, 7: 627–643.
[10] J P Liu, W X Zheng, Y Zheng. Research on the relevance of AEB system performance and TTC. *Automobile Technology*, 2018, 8: 51–53.
[11] L Xiong, M Liu, X Yan, et al. Integrated path tracking for autonomous vehicle collision avoidance based on model predictive control with multi-constraints. *Proceedings of the International Conference on Intelligent Transportation Systems (ITSC)*, 2022: 554–561.
[12] S Müller, T Raste. *Future brake systems and motion control. in next generation electrified vehicles optimised for the infrastructure*. Cham: Springer Nature Switzerland, 2024.
[13] X K He, Y L Liu, C Lv, et al. Emergency steering control of autonomous vehicle for collision avoidance and stabilisation. *Vehicle System Dynamics*, 2018, 57(8): 1163–1187.
[14] N Fricke, S Griesche, A Schieben, et al. Driver behavior following an automatic steering intervention. *Accident Analysis & Prevention*, 2015, 83: 190–196.
[15] Z Zhao, L Zhang, X L Ding, et al. Integrated active suspension and anti-lock braking control for four-wheel-independent-drive electric vehicles. *Chinese Journal of Mechanical Engineering*, 2024, 37: 20.
[16] Z P Wang, G B Li, H J Jiang, et al. Collision-free navigation of autonomous vehicles using convex quadratic programming-based model

predictive control. *IEEE/ASME Transactions on Mechatronics*, 2018, 23(3): 1103–1113.
[17] J Shah, M Best, A Benmimoun, et al. Autonomous rear-end collision avoidance using an electric power steering system. *Proceedings of the Institution of Mechanical Engineers, Part D: Journal of Automobile Engineering*, 2015, 229(12): 1638–1655.
[18] J H Guo, P Hu, R B Wang. Nonlinear coordinated steering and braking control of vision-based autonomous vehicles in emergency obstacle avoidance. *IEEE Transactions on Intelligent Transportation Systems*, 2016, 17(11): 3230–3240.
[19] A Seewald, C Haß, M Keller, et al. Emergency steering assist for collision avoidance. *ATZ Worldwide*, 2015, 117(1): 14–19.
[20] X W Ji, K M Yang, X X Na, et al. Shared steering torque control for lane change assistance: A stochastic game-theoretic approach. *IEEE Transactions on Industrial Electronics*, 2018, 66(4): 3093–3105.
[21] Y Liu, Q Xu, H Y Guo, et al. A type-2 fuzzy approach to driver-automation shared driving lane keeping control of semi-autonomous vehicles under imprecise premise variable. *Chinese Journal of Mechanical Engineering*, 2022, 35: 46.
[22] M J Li, C Jiang, X L Song, et al. Parameter effects of the potential-field-driven model predictive controller for shared control. *Automotive Innovation*, 2023, 6: 48–61.
[23] D J Song, B Zhu, J Zhao, et al. Human–machine shared lateral control strategy for intelligent vehicles based on human driver risk perception reliability. *Automotive Innovation*, 2024, 7: 102–120.
[24] M J Li, H T Cao, X L Song, et al. Shared control driver assistance system based on driving intention and situation assessment. *IEEE Trans. Ind. Informat*., 2018, 14(11): 4982–4994.
[25] A Bemporad, M Morari. Control of systems integrating logic, dynamics, and constraints. *Automatica*, 1999, 35(3): 407–427.
[26] D Tran, J Du, W Sheng, et al. A human-vehicle collaborative driving framework for driver assistance. *IEEE Transactions on Industrial Informatics*, 2018, 20(9): 3470–3485.
[27] L Zhang, Z Q Zhang, Z P Wang, et al. Chassis coordinated control for full x-by-wire vehicles-A review. *Chinese Journal of Mechanical Engineering*, 2021, 34: 42.
[28] J Thunberg, D Bischoff, F A.Schiegg, et al. Unreliable V2X communication in cooperative driving: Safety times for emergency braking. *IEEE Access*, 2021, 9: 148024–148036.
[29] G van Lookeren Campagne, D Yang. A nonlinear model predictive control based evasive manoeuvre assist function. *IAVSD International Symposium on Dynamics of Vehicles on Roads and Tracks,* Cham: Springer International Publishing, 2021.
[30] S Q Li, Q Q Zhao. Research on the emergency obstacle avoidance strategy of intelligent vehicles based on a safety distance model. *IEEE Access*, 2023, 11: 7124–7134.
[31] L Saleh, P Chevrel, F Claveau, et al. Shared steering control between a driver and an automation: stability in the presence of driver behavior uncertainty. *IEEE Transactions on Intelligent Transportation Systems*, 2013, 14(2): 974–983.
[32] Z R Li, J Hu, B Leng, et al. An integrated decision making and motion planning framework for enhanced oscillation-free capability. *IEEE Transactions on Intelligent Transportation Systems*, 2024, 25(6): 5718–5732.
[33] X Wang, Q Wang, Z Gao, et al. Man-machine shared driving based lane departure avoidance control. *Automotive Engineering*, 2017, 39(7): 839–848.
[34] K Iwano, P Raksincharoensak, M Nagai. A study on shared control between the driver and an active steering control system in emergency obstacle avoidance situations. *Proceedings of IFAC*, 2014, 47(3): 6338–6343.
[35] Z P Yu, Y Y Hou, B Leng, et al. Disturbance compensation and torque coordinated control of four in-wheel motor independent-drive electric vehicles. *IEEE Access*, 2020, 8: 119758–119767.

Bo Leng born in 1991, received the Ph.D. degrees in vehicle engineering from *Tongji University, China*, in 2019. He is currently working as an associate professor at *School of Automotive Studies, Tongji University, China*. He mainly engages in researches on dynamic control of distributed drive electric vehicles, and motion planning and control of intelligent vehicles. He has won the first prize of China Automobile Industry Technology Invention Award, the First Prize of Shanghai Science and Technology Progress Awards in 2020 and 2022, respectively; and has been selected into the Young Elite Scientists Sponsorship Program of China Association for Science and Technology in 2022

Zhuoren Li born in 1996, received the B.E. degree from *School of Aerospace Engineering and Applied Mechanics, Tongji University, China*, in 2019. He is currently pursuing his Ph.D. degree with *the School of Automotive Studies, Tongji University, China*. His research interests include interaction decision making, motion planning, and safe reinforcement learning of autonomous vehicles.

Ming Liu born in 1997, received his B.Eng. in mechanical design, manufacture and automation from *Hunan University, China*, in 2019. He is currently pursuing his Ph,D. degree with the *School of Automotive Studies, Tongji University, China*. His research interests include vehicle dynamics and control and intelligent vehicle trajectory motion control.

Ce Yang born in 1996, received his B.S. degree in vehicle engineering from the *School of Mechanical and Vehicle Engineering, Chongqing University, China*, in 2018. And then he received his M.S. degree in vehicle engineering from *Tongji University, China*, in 2021. His research interests include motion planning and model predictive control.

Yi Luo graduated in electronics engineering from the *University of Electronic Science and Technology of China*. He has worked in the electronic power-steering field for more than 15 years and is currently a leader of the Intelligent-Steering-System BU in the *DIAS Automobile Electronics Co., Ltd*., *China*.

Amir Khajepour born in 1967, received the Ph.D. degree from the *University of Waterloo*, *Canada*, in 1996. is a Professor of mechanical and mechatronics engineering and the Director of the *Mechatronic Vehicle Systems (MVS) Laboratory, University of Waterloo*, *Canada*. He held the Tier 1 Canada Research Chair in mechatronic vehicle systems (2008–2022) and the Senior NSERC/General Motors Industrial Research Chair in holistic vehicle control (2017–2022). His work has led to the training of over 150 Ph.D. and M.A.Sc. students, filing of 30 patents, publication of 600 research papers, numerous technology transfers, and the establishment of several start-up companies. He is a fellow of the Engineering Institute of Canada, the American Society of Mechanical Engineering, and the Canadian Society of Mechanical Engineering. He has been recognized with the Engineering Medal from Professional Engineering Ontario.

Lu Xiong born in 1978, received the Ph.D. degree in vehicle engineering from *Tongji University, China*, in 2005. He is currently the vice president and professor with the *School of Automotive Studies, Tongji University, China*. Dr. Xiong won the first prize of Shanghai Science and Technology Progress Awards in 2013, 2019 and 2022. He was the recipient of the National Science Fund for Distinguished Young Scholars. His research interests include dynamic control of distributed drive electric vehicles, motion planning and control of intelligent vehicles, and all-terrain vehicles.